GSA DATA REPOSITORY 2014319

Mesalles et al.

Zircon fission-track method and data

Sample processing and ZFT analysis were performed at the thermochronology laboratory of ISTerre (Université Joseph Fourier). We used standard ZFT preparation procedures (Bernet and Garver, 2005). In addition, for each sample two to three different Teflon mounts were prepared and etched for different lengths of time, ranging from 15h to 56h, ensuring proper etching for variable radiation damage zircon populations.

In contrast to other studies, we use young-peak ages (YPA) in the vertical profiles when more than one population exists instead of pooled ages (Table DR1 and DR2). The reason behind this choice lies on the thermal stability of ZFT, which is dependent on single grain radiation damage. Zircons in detrital suites are known to have a wide range of radiation damage due to the varied source thermal history and Uranium and Thorium content. This implies different closure temperature for the different radiation damaged populations, with low-retentive zircons (i.e. high radiation damage) annealing at low temperature of about 180-200°C (Brandon et al., 1998; Garver et al., 2005) and high retentive zircons (i.e. with low radiation damage) annealing at higher temperature of about ~280-300°C (Garver et al., 2005), or for the rapidly exhuming Taiwan orogen ~260ºC (Liu et al., 2001).

In our study, we observed that most of the higher altitude samples (above the break-in-slope at ~1500m; Fig. 2A) present a young peak age younger than the depositional age (Table DR2). As discussed in the main text our data and interpretation support that the young peak zircon population is a reset low-retention zircon population having reached 180-200°C. On the other hand, most of the lower samples present a single young age population (Table DR1) indicating that all zircon populations have been reset and may have reached temperatures in excess of ~260ºC. The young peak populations are interpreted to record the last thermal event and, thus, the age-elevation trend observed in the profile reflects cooling rate. Hence, the ZFT partial annealing zone concept is probably inappropriate in our case. The low retentive zircon grains have very likely been totally annealed and thus have not kept any record of its previous history as implied by the partial annealing zone concept.

Age populations deconvolution was extracted using Binomfit 1.2.60 (Brandon, 1992).

Apatite fission-track method and data

We used standard AFT preparation procedures (Donelick et al., 2005). Results were obtained from the conglomeratic samples of the Linkou and Liukuei formations and presented very low spontaneous and induced track counts with some grains presenting up to zero effective uranium content (Figure DR1 and Table DR4). Conversely to the ZFT ages presented in Fig.3, AFT samples from the Linkou and Liukuei were merged together as the number of counted grains did not allow to reliably extract detrital age populations for the two conglomerates separately.

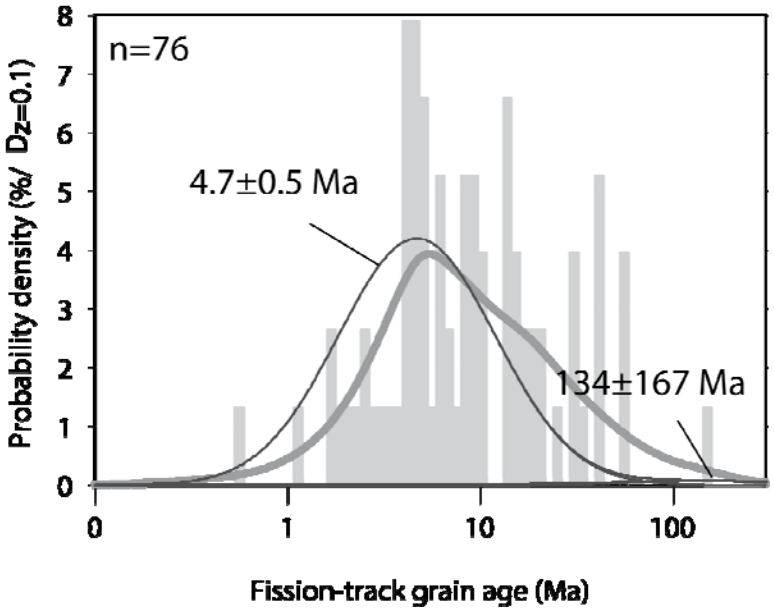

Figure DR1 : AFT grain-age probability-density plot and distribution histogram with binomial fitted peaks (thin black line) of the Linkou and Liukuei samples all together (see Table DR4). Thick gray line represents observed probability grain-age distribution.

Age populations deconvolution was extracted using Binomfit 1.2.60 (Brandon, 1992).

Inverse modeling approach

To gain a better understanding of the effects of heat advection due to erosion rate changes and dependence of closure temperature on cooling rates, we performed inverse modelling of our ZFT age-elevation profile data presented in Figure 2A. We adopted the analytical solution proposed by Willett and Brandon (2013) that uses the time-dependant eroding half-space thermal model solution. In our case, this solution is particularly useful to extract exhumation rates in the lower part of the profile (from 465 to 1324 m) where the ages remain constant and no age-elevation relationship (AER) can be extracted directly from the age-elevation plot, or through classical thermal models (e.g., Gallagher, 2012; Braun et al., 2012).

The results are highly sensitive to the initial geothermal gradients and to a lesser degree to the time of initiation of exhumation of the studied phase. The model requires choosing a time of initiation of exhumation slightly older than the oldest modelled sample. We choose 7.2 Ma and 3.7 Ma as the time for initiation of cooling for the upper and lower parts of the profile, respectively.

Although there is no single crossing point of all the age-curves in the age-function plots, as expected for perfectly linear AER, the models show convergence in an area supporting exhumation rates of 1.2 to 2.2 km/m.y. (1.7 km/m.y. on average) with geothermal gradients of 60 to 70ºC/km for the lower section of the profile (Figure 2B), and of 0.4 to 1.16 km/Myr

(0.78 km/m.y. on average) with geothermal gradients of 36 to 46ºC/km, for the upper section of the profile (Figure 2C). The choice of this optimal inverse model was done based on the range of geothermal gradients that produced the narrower range of exhumation rates.

A surface temperature of 15^{o}C and a mean elevation of 939 m in the sample area vicinity (mean elevation for a 20km radius of the sampled area) were adopted, using the annealing parameters of Brandon et al. (1998). The geothermal gradient values seem to be in agreement with present-day geotherms for the younger phase, and with present-day geotherms offshore southern Taiwan for the older phase (Chi and Reed, 2008), as discussed in the main text.

We acknowledge that our inverse model do not take into account the full range of physical processes taking place in natural submarine orogenic wedges. These are, for instance, underwater fluid circulation effect on the thermal structure or underwater surface temperature. However, because our first cooling phase (~7.1 to ~3.2 Ma) that initiated underwater also comprises a subaerial stage (~5 to ~3.2Ma), the adopted subaerial boundary conditions are probably a good approximation of the complex evolution of natural orogenic/submarine tectonic systems.

Forward modeling

To independently represent the cooling history inferred from inverse modeling and test the fit with ZFT age variations from the age-elevation profile, we forward modeled time-temperature history and calculated synthetic profiles of age versus elevation using HeFTy v.1.8.0 (Ketcham, 2005). In the new release of the HeFTy software, ZFT annealing models of Rahn et al. (2004),Yamada et al. (2007) and Ketcham et al. (unpublished) are incorporated. For modeling, we tested different annealing parameters and finally retained the fanning model (Yamada et al., 2007), as it best fits our data, probably due to the high cooling rate involved, and therefore the high closure temperature necessary to reproduce our data.

To explore the time-temperature space using the prescribed scenario of exhumation given by the inverse model, all samples positioned at different elevation, or paleo-depth in a column of rocks, were subjected to the same thermal history. We ran forward models offset by 10°C increments to simulate time-temperature history and obtain ZFT age at different depths. The thermal model assumed isothermal holding from 30 Ma (Oligocene) to Late Miocene that reproduces post-break-up evolution recognized offshore Taiwan in the SCS margin (Lin et al., 2003). To obtain the final age-elevation plot of Figure 2, we converted time-temperature paths obtained for intervals at 30-7.2 Ma, 7.2-3.7 and 3.7-0 Ma to time-elevation using geothermal gradients of 36°C/km before 3.7 Ma and 70°C/km after, in agreement with inverse modeling. The initial gradient of 36°C/km is consistent with current values reported in the accretionary prism offshore southern Taiwan (Chi and Reed, 2008). After 3.7 Ma, the geothermal gradient of 70°C/km reflects efficient advection of heat enhanced by coupling between tectonics and surface processes and is also consistent with current values determined in central Taiwan (Chi and Reed, 2008).

Our preferred forward model, as shown in Fig. 2, was established for three successive cooling periods at 30-7.2 Ma, 7.2-3.7 Ma and 3.7-0 Ma. Slow cooling from Oligocene to Late Miocene is intended to reproduce post-break-up thermal evolution recognized offshore Taiwan in the SCS margin, which is associated with thermal subsidence (Lin et al., 2003).

Table DR1: ZFT counting data and pooled ages for all samples in this study. Concordant ages present a single population of fully reset zircons. Discordant ages (†) are presented in Table DR2. N: Total number of counted grains. U: Uranium content given with two standard deviations. ρ_S and N_S, density and number of spontaneous fission tracks, respectively. ρ_i and N_i, density and number of induced fission tracks. ρ_d and N_d., density and number of measured in fluence dosimeter. Extracted with Binomfit 1.2.60 (Brandon, 1992).

Name	Lon(°E)	Lat(°N)	Alt (m)	ρ_s (10^5 tracks . cm^{-2})	Ns (tracks)	ρ_i (10^6tracks . cm^{-2})	Ni (track)	U±2s (ppm)	N	Grain-age Range (Ma)	Pooled age ±1σ (Ma)
Ph0	120.823	22.576	465	6.83	151	3.72	823	181±39	24	1.7-8.7	**3.4 ±0.5**
PV1-2B	120.837	22.597	467	3.98	83	2.39	497	129±12	24	1.4-7.2	**3.1±0.6**
PV3-7	120.804	22.604	596	5.92	169	3.34	955	181±12	24	1.4-7.1	**3.3±0.5**
PV1-3	120.827	22.605	680	4.13	123	2.7	804	147±11	38	1.4-18.7	**2.9±0.5**
PV1-5	120.825	22.613	1122	4.86	81	2.51	419	136±14	24	1.4-8.7	**3.6±0.7**
PV1-6	120.826	22.615	1324	3.79	54	2.51	358	136±15	23	1.4-8	**2.8±0.6**
PV3-1	120.784	22.637	1728	5.92	107	2.06	372	112±12	24	2.5-26.5	**5.4±0.9**
PV3-6B †	120.805	22.621	709	5.60	131	2.49	582	135±12	24	2.2-15.1	**4.2±0.7 †**
PV4-3 †	120.747	22.614	2468	16.8	298	1.56	277	85±10	25	5.6-59.5	**20.1±3.0 †**
PV4-1 †	120.754	22.617	2867	20.0	337	1.98	334	108±12	24	3.7-96.9	**18.8±2.8 †**
PV4-0 †	120.756	22.619	3004	26.3	549	2.04	427	111±11	24	2.8-97.0	**24.0±3.3 †**
PV3 †	120.761	22.627	3095	13.2	264	1.90	381	103±11	24	3.2-64.2	**12.9±1.9 †**

Table DR2: Discordant ZFT ages in which population 1 (P1) is interpreted as a reset low-retention zircon population. Note the generally higher uranium content of P1 compared to the whole sample uranium content (Table DR1). N: Total number of counted grains; binomial peak fitting are given ± 1σ. Also given is the percentage of grains for a specific peak. All samples were counted by Lucas Mesalles using a zeta of 135.42 ± 15.20. The probability based on F-test evaluates significance of number of peaks. A probability of 0% indicates that the introduction of additional peaks would result in the decrease of the best-fitting solution. Extracted with Binomfit 1.2.60 (Brandon, 1992).

									ZFT age components ±1σ		
Name	Position	Lon (°E)	Lat (°N)	Elevation (m)	N	Grain-age Range (Ma)	F test (%)	P1's U ±2s (ppm)	P1 (Ma)	P2 (Ma)	P3 (Ma)
PV3-6B	Eastern Divide	120.805	22.621	709	24	2.2-15.1	0	155±14	**3.3±0.6 (75%)**	**8.6±2.6 (25%)**	
PV4-3	Western divide	120.747	22.614	2468	25	5.6-59.5	0	91±14	**13.2±2.3 (77%)**	**47.7±12 (23%)**	
PV4-1	Western divide	120.754	22.617	2867	24	3.7-96.9	0	111±22	**5.3±2.2 (19%)**	**14±2.7 (28%)**	**32.2±6.2 (53%)**
PV4-0	Crest	120.756	22.619	3004	24	2.8-97.0	0	131±31	**6.6±4.7 (19%)**	**27.2±4 (81%)**	
PV3	Crest-Peak	120.761	22.627	3095	24	3.2-64.2	0	115±14	**7.1±1.3 (61%)**	**29.1±5.7 (39%)**	

Table DR3: Detrital zircon fission-track data in Nanshihlun Sandstones, and Linkou and Liukuei conglomerates. N: Total number of counted grains; binomial peak fitting are given ± 1σ. Also given is the percentage of grains for a specific peak. All samples were counted by Lucas Mesalles using a zeta of 135.42 ± 15.20. In the text, we refer only to populations that are close to or above 30%. Extracted with Binomfit 1.2.60 (Brandon, 1992).

									ZFT age components ±1σ			
Sample	Formation	Depositional age	Lon(°E)	Lat(°N)	Alt (m)	N	age range (Ma)	F test (%)	P1 (Ma)	P2 (Ma)	P3 (Ma)	P4 (Ma)
NA02	Nanshihlun sandstones	NN15 (~3.8-4Ma)	120.3957062	22.7341431	124	84	21.1-781.3	0	**22.9±6.5 (3%)**	**59±8.3 (42%)**	**136.8± 21.6 (47%)**	**395.7± 213 (8%)**
LK03	Linkou Fm (base Lower member)	NN19 (~1.8-2 Ma)	120.4042457	22.7383202	119	190	1.2-186.8	0	**4.7±0.7 (32.2%)**	**66±8.2 (67.8%)**		
LK04	Linkou Fm (top Upper member)	n.a.	120.4204844	22.6992047	53							
LK15	Liukuei Fm	n.a.	120.6424799	22.9383224	203	332	0.8-599.8	0	**6.3±0.8 (28.4%)**	**47.5±6.2 (40.6%)**	**102.9± 14.9 (31%)**	
LK17			120.6365015	22.9315449	250							
LK18			120.6192217	22.911682	155							
LK20			120.6357397	22.9393456	227							

Table DR4: Detrital apatite fission-track data from the Linkou and Liukuei conglomerates. N: Total number of counted grains; binomial peak fitting are given ± 1σ. Also given is the percentage of grains for a specific peak. All samples were counted by Lucas Mesalles using a zeta of 268.37 ± 7.61. In the text, we refer only to populations that are close to or above 30%. Extracted with Binomfit 1.2.60 (Brandon, 1992).

				AFT age components ±1σ	
Sample	N	Grain-age range (Ma)	Prob F test (%)	P1 (Ma)	P2 (Ma)
LK03	76	0.6-144	0	**4.7±0.5 (98%)**	**134.6±167 (2%)**
LK04					
LK15					
LK17					
LK18					
LK20					

References

Bernet, M., and Garver, J.I., 2005, Fission-track analysis of detrital zircon, Low-temperature thermochronology: techniques, interpretations, and applications Volume 58: Reviews in mineralogy & geochemistry, Mineralogical Society of America, p. 205-237.

Brandon, M.T., 1992, Decomposition of fission-track grain-age distributions: American Journal of Science, v. 292, p. 535-564.

Brandon, M.T., Roden-Tice, M.K., and Garver, J.I., 1998, Late Cenozoic exhumation of the Cascadia accretionary wedge in the Olympic Mountains, northwest Washington State: Geological Society of America Bulletin, v. 110, p. 985-1009.

Braun, J., van der Beek, P. Valla, P., Robert, X., Herman, F., Glotzbach, C., Pedersen, V., Perry, C., Simon-Labric, T. and Prigent, C., 2012, Quantifying rates of landscape evolution and tectonic processes by thermochronology and numerical modeling of crustal heat transport using PECUBE, Tectonophysics, v. 524-525, p. 1–28, doi:10.1016/j.tecto.2011.12.035.

Chi, W.-C., and Reed, D. L., 2008. Evolution of shallow, crustal thermal structure from subduction to collision: An example from Taiwan. Geological Society of America Bulletin, v.120(5-6), p. 679–690.

Donelick, R. A., O'Sullivan, P. B., and Ketcham, R. A., 2005. Apatite Fission-Track Analysis. Reviews in Mineralogy and Geochemistry, v. 58(1), p. 49–94.

Gallagher, K., 2012, Transdimensional inverse thermal history modeling for quantitative thermochronology, Journal of Geophysical Research, v. 117(B2), p. 1–16, doi:10.1029/2011JB008825.

Garver, J., Reiners, P., Walker, L.J., Ramage, J., and Perry, S., 2005, Implications for timing of Andean uplift from thermal resetting of radiation□damaged zircon in the Cordillera Huayhuash, Northern Peru: The Journal of Geology, v. 113, p. 117-138.

Ketcham, R.A., 2005 Forward and inverse modeling of low-temperature thermochronometry data: Reviews in Mineralogy & Geochemistry, v. 58, p. 275–314.

Kirstein, L. A., M. G. Fellin, S. D. Willett, A. Carter, Y.-G. Chen, J. I. Garver, and D. C. Lee , 2009, Pliocene onset of rapid exhumation in Taiwan during arc-continent collision: new insights from detrital thermochronometry, Basin Research, v. 22(3), p. 270–285.

Kirstein, L. A., A. Carter, and Y.-G. Chen, 2010, Testing inferences from palaeocurrents: application of zircon double-dating to Miocene sediments from the Hengchun Peninsula, Taiwan, Terra Nova, 22(6), p. v. 483–493.

Lin, A.T., Watts, A.B., and Hesselbo, S.P., 2003, Cenozoic stratigraphy and subsidence history of the South China Sea margin in the Taiwan region: Basin Research, v. 15, p. 453-478.

Liu, T.-K., Hsieh, S., Chen, Y.-G., and Chen, W.-S., 2001, Thermo-kinematic evolution of the Taiwan oblique-collision mountain belt as revealed by zircon fission track dating: Earth and Planetary Science Letters, v. 186, p. 45–56, doi:10.1016/S0012-821X(01)00232-1.

Rahn, M.K., Brandon, M.T., Batt, G.E., and Garver, J.I., 2004, A zero-damage model for fission-track annealing in zircon: American Mineralogist, v. 89, p. 473-484.

Willett, S.D., and Brandon, M.T., 2013, Some analytical methods for converting thermochronometric age to erosion rate: Geochemistry, Geophysics, Geosystems, v. 14, p. 209-222, 10.1029/2012gc004279.

Yamada, R., Murakami, M., and Tagami, T., 2007, Statistical modelling of annealing kinetics of fission tracks in zircon; Reassessment of laboratory experiments: Chemical Geology, v. 236, p. 75-91.

Yamato, P., Mouthereau, F., and Burov, E., 2009, Taiwan mountain building: insights from 2D thermo-mechanical modelling of a rheologically-stratified lithosphere: Geophysical Journal International, v. 176, p. 307-326.